J. Plasma Physics (2009), *vol.* 75, *part* 3, *pp.* 359–371.

doi:10.1017/S0022377808007666 Printed in the United Kingdom

Magnetic detachment and plume control in escaping magnetized plasma

P. F. SCHMIT and N. J. FISCH

Department of Astrophysical Sciences, Princeton University, Princeton, NJ 08540, USA (pschmit@princeton.edu)

(Received 17 June 2008 and accepted 20 September 2008, first published online 14 November 2008)

Abstract. The model of two-fluid, axisymmetric, ambipolar magnetized plasma detachment from thruster guide fields is extended to include plasmas with non-zero injection angular velocity profiles. Certain plasma injection angular velocity profiles are shown to narrow the plasma plume, thereby increasing exhaust efficiency. As an example, we consider a magnetic guide field arising from a simple current ring and demonstrate plasma injection schemes that more than double the fraction of useful exhaust aperture area, more than halve the exhaust plume angle, and enhance magnetized plasma detachment.

1. Introduction

Many electric propulsion schemes involve magnetized plasma escaping from a magnetic guide field acting as an effective nozzle. One of the central problems in ensuring the efficient conversion of exhaust momentum into useful thrust with these systems is magnetized plasma detachment. Applied magnetic fields within the thruster tend to confine one or both of the plasma constituents. Thus, the tendency for the plasma to flow along the closed field lines means that unless sufficient cross-field flux or magnetic field distortion and reconnection occurs in the exhaust plume, momentum will not be transferred to the spacecraft. Furthermore, plasma that does manage to cross flux surfaces and escape confinement becomes defocused by the physical dipole structure of the external nozzle guide field, and so questions arise as to how to exploit the benefits of a magnetic guide field for electrically quasineutral plasmas while avoiding the issues of plasma trapping and plume defocusing.

Several models have been proposed to describe the physics of magnetic plasma detachment [1–4]. Arefiev and Breizman describe magnetized ideal MHD flow constrained to be field-directed everywhere and characterize successful detachment by the transition of plasma flow from a sub-Alfvénic to a super-Alfvénic regime [1, 2]. Physically, the detached plume is said to stretch the frozen-in magnetic field lines to infinity. Gesto et al. [4] describe detachment by analyzing single ion kinetics in the axisymmetric, solenoidal vacuum guide field of the Helicon Double-Layer Thruster (HDLT), ignoring electron dynamics and the effects of an ambipolar electric field between the species and presuming the exhaust plume is charge-neutralized. Detachment is defined as the asymptotic approach toward zero of the ion trajectory curvatures in the r–z plane. In contrast, Hooper [3] characterizes plasma detachment by giving an approximate model for the ambipolar drift of a two-fluid plasma across magnetic flux surfaces. The model does not constrain the plasma to flow along field lines but provides a necessary condition

for the plasma streamline to be able to escape to infinity. Hooper suggests that this process is generally inefficient, allowing only miniscule utilization of the entire exhaust aperture to produce directed flow in some experimentally relevant cases. However, Hooper restricts his analysis to a cold, field-directed initial flow in order to arrive at these conclusions.

We adopt Hooper's model and expand its use to include plasma flows with non-zero injection angular velocity profiles. In generalizing his approach to include such flows, we demonstrate that it is possible simultaneously to enhance detachment, narrow the exhaust plume, and increase the exhaust aperture utilization. This is accomplished by adding an initial angular velocity profile to the plasma at the system boundary.

In Sec. 2 we derive the relevant generalized equations of motion for a cold, locally quasineutral two-fluid plasma flow, adopting the same method of characteristics used by Hooper in the more restricted case of axially directed initial flow. Then, in Sec. 3, we cast these equations into a physically intuitive form, which will suggest guidelines for choosing rotational injection profiles that will enhance thruster performance and detachment. In Sec. 4, we follow Hooper and apply this generalized model to the example of a current ring guide field to demonstrate the substantial performance improvements a rotating flow can produce compared to purely axial flow. Finally, in Sec. 5, we discuss the relevance of our results with respect to current thruster experiments and describe briefly the physics of a few methods for generating rotating columnar plasma flows.

2. Derivation of equations of motion

Following Hooper, begin by assuming a cold, collisionless, two-fluid plasma in an axisymmetric, externally applied magnetic guide field and examine the steady-state solutions for a magnetized flow [3]. Each species obeys the non-relativistic fluid field equations for continuity and momentum balance:

$$\nabla \cdot (n_\alpha \mathbf{u}_\alpha) = 0, \tag{2.1}$$

$$\mathbf{u}_\alpha \cdot \nabla \mathbf{u}_\alpha = (q_\alpha / m_\alpha)(\mathbf{E} + \mathbf{u}_\alpha \times \mathbf{B}). \tag{2.2}$$

We examine the class of steady-state solutions that are locally quasineutral. This amounts to the assumption that the two plasma species injected along the system boundary have equal densities, while the condition

$$\tilde{\mathbf{j}} = 0 \tag{2.3}$$

holds throughout the plasma and along the boundary. Here $\tilde{\mathbf{j}}$ signifies the plasma current in the r–z plane, and the tilde notation will be used throughout as a label for r–z, or meridional, vector quantities. Note that (2.3) implies that $\tilde{\mathbf{u}}_\alpha$ is the same for electrons and ions in a singly ionized plasma species, and thus the electron and ion velocity fields are identical except in the azimuthal direction, where the electron and ion species can have different velocities in general.

Since we are working with a static, axisymmetric magnetic field, $\mathbf{B}$ can be written as

$$\mathbf{B} = -\frac{\hat{\theta} \times \tilde{\nabla}\Psi}{r}, \tag{2.4}$$

where $\Psi(r, z) = rA_\theta$ is the magnetic flux function. We will assume that the plasma couples negligibly with the magnetic field via the azimuthal current.

https://doi.org/10.1017/S0022377808007666 Published online by Cambridge University Press

Equation (2.2) can be broken up into its meridional and azimuthal vector components:

$$\tilde{\mathbf{u}}_\alpha \cdot \tilde{\nabla}\tilde{\mathbf{u}}_\alpha = \frac{q_\alpha}{m_\alpha}(\mathbf{E} + \mathbf{u}_{\alpha\theta} \times \mathbf{B}) + \frac{\mathbf{u}_\theta^2}{r}\hat{\mathbf{r}} \tag{2.5}$$

$$\tilde{\mathbf{u}}_\alpha \cdot \tilde{\nabla}(m r u_{\alpha\theta} + q\Psi) = 0. \tag{2.6}$$

We recognize (2.6) as a statement of conservation of canonical angular momentum along streamlines. This system of equations lends itself to solution by the method of characteristics, where we choose the parameterization

$$\frac{dr}{dt} = u_r, \quad \frac{dz}{dt} = u_z.$$

Note that the characteristic curves of this quasilinear system of equations simultaneously specify the meridional plasma streamlines. A quasilinear first-order system of equations is linear in the derivatives of the dependent variables, in this case the r- and z-components of $\tilde{\mathbf{u}}_\alpha$, but nonlinear with respect to the dependent variables themselves. We can solve immediately for the azimuthal velocity along each characteristic curve:

$$u_{\alpha\theta} = \frac{q_\alpha}{m_\alpha}\frac{P_{\alpha\theta}/q_\alpha - \Psi}{r}, \tag{2.7}$$

where $P_{\alpha\theta} = m_\alpha r_0 u_{\alpha\theta 0} + q_\alpha \Psi(r_0, z_0 = 0)$ corresponds to the local particle canonical angular momentum at the point of injection along the system boundary. Hooper solves the problem where $u_{\alpha\theta 0} = 0$, in which case $P_{\alpha\theta}/q_\alpha = \Psi(r_0, z_0 = 0) \equiv \Psi_0$. We will relax these conditions and allow for each species to be given non-zero initial azimuthal velocity.

Having reduced the number of independent spatial degrees of freedom of the system to two, we can derive an equation of motion for the fluid in a very intuitive form first by inserting (2.7) into (2.5) and then combining the resulting electron and ion equations, since their meridional velocities are defined to be identical in the regime of interest. For notational simplicity we define $P_{\alpha\theta}/q_\alpha \equiv \Psi'_{\alpha 0}$, which has units of magnetic flux. Representing $\mathbf{B}$ by the result of (2.4), we find

$$\tilde{\mathbf{u}}_\alpha \cdot \tilde{\nabla}\tilde{\mathbf{u}}_\alpha = \frac{q_\alpha}{m_\alpha}\mathbf{E} + \frac{q_\alpha^2}{m_\alpha^2}\left(\frac{-\hat{\theta} \times (\hat{\theta} \times \tilde{\nabla}\Psi)(\Psi'_{\alpha 0} - \Psi)}{r^2} + \frac{(\Psi'_{\alpha 0} - \Psi)^2}{r^3}\hat{r}\right).$$

Further reduction yields

$$\tilde{\mathbf{u}}_\alpha \cdot \tilde{\nabla}\tilde{\mathbf{u}}_\alpha = \frac{q_\alpha}{m_\alpha}\mathbf{E} - \frac{q_\alpha^2}{m_\alpha^2}\tilde{\nabla}\left(\frac{(\Psi'_{\alpha 0} - \Psi)^2}{2r^2}\right). \tag{2.8}$$

Here we make our first explicit use of the local quasineutrality condition $\tilde{\mathbf{j}} = 0$, which requires that the meridional fluid velocities for both species be identical, or $\tilde{\mathbf{u}}_\mathrm{i} = \tilde{\mathbf{u}}_\mathrm{e} = \tilde{\mathbf{u}}$. We multiply each species' equation by m_α and add the two equations together to find

$$\tilde{\mathbf{u}} \cdot \tilde{\nabla}\tilde{\mathbf{u}} = -\tilde{\nabla}\left(\frac{e^2(m_\mathrm{e}(\Psi'_{\mathrm{i}0} - \Psi)^2 + m_\mathrm{i}(\Psi'_{\mathrm{e}0} - \Psi)^2)}{2m_\mathrm{i}m_\mathrm{e}(m_\mathrm{i} + m_\mathrm{e})r^2}\right). \tag{2.9}$$

We have assumed a singly ionized ion species in arriving at the above equation. Recalling that we are solving for the plasma flow along the characteristic curves following the parameterization specified above, we note the equivalence of the two

https://doi.org/10.1017/S0022377808007666 Published online by Cambridge University Press

expressions

$$\tilde{\mathbf{u}} \cdot \tilde{\nabla} \tilde{\mathbf{u}} \Leftrightarrow \frac{d\tilde{\mathbf{u}}}{dt}, \tag{2.10}$$

and thus the problem of solving for the plasma streamlines and corresponding flow velocities is isomorphic to the problem of solving for the trajectories and velocities of a single particle with hybrid mass $(m_\mathrm{i} m_\mathrm{e})^{1/2}$ in a two-dimensional effective potential

$$U_\mathrm{eff} = \frac{e^2 (m_\mathrm{e} (\Psi'_{\mathrm{i}0} - \Psi)^2 + m_\mathrm{i} (\Psi'_{\mathrm{e}0} - \Psi)^2)}{2(m_\mathrm{i} m_\mathrm{e})^{1/2} (m_\mathrm{i} + m_\mathrm{e}) r^2}. \tag{2.11}$$

This generalized form for U_eff reduces to Hooper's result, defined in (3.1), in the limit of zero initial azimuthal rotation.

3. Detachment and general effects of azimuthal rotation

First, we address Hooper's limit, in which neither plasma species is given any initial rotation [3]. In this case, referring to (2.9) through (2.11), we see that $\Psi'_{\mathrm{i}0} = \Psi'_{\mathrm{e}0} = \Psi_0$, and the characteristic equation simplifies to

$$m_h \frac{d\mathbf{u}}{dt} = -\nabla \left(\frac{e^2 (\Psi_0 - \Psi)^2}{2 m_h r^2} \right) \equiv -\nabla U_\mathrm{H}, \tag{3.1}$$

where $m_h \equiv (m_\mathrm{i} m_\mathrm{e})^{1/2}$, and U_H is the effective r–z potential in Hooper's limit. Also, the tildes have been omitted, and it is understood that $\mathbf{u}$ occupies the two-dimensional r–z vector subspace of the three-dimensional system. Note that (3.1) is exactly the same as the differential equation that determines the r–z space trajectory of a particle of mass m_h moving in the same static externally applied field as that of the original plasma problem. Thus we can picture how the presence of two neutralizing species affects the detachment phenomenon: the heavy ions effectively increase the apparent cross-field transport of electrons while the relatively strong confinement of the lighter electrons serves to decrease the effective inertial mass of the ions and tie them to the magnetic field, with the effect communicated between species by local microscopic ambipolar electric fields.

Note that, by the assumptions of local quasineutrality and equal densities of both species at the injection surface, no macroscopic electric self-field can arise in this system. Thus it may seem unnecessary to add the fluid equations for the two different species together to eliminate $\mathbf{E}$, since by design our plasma has no macroscopic electric field and $\mathbf{E} = 0$. Local quasineutrality reduces the velocity space degrees of freedom in our system from four to two, and thus we must combine the electron and ion fluid equations to form a single two-dimensional vector field equation for the two remaining degrees of freedom in our system. Adding the two mass-scaled fluid equations together and enforcing local quasineutrality takes advantage of the canceling responses of the two species in the presence of *any* macroscopic electric field.

The form of the effective potential implied in (3.1) provides a very intuitive visualization of a well-confined trajectory: U_H is positive definite, and it only equals zero when the particle lies on its initial flux surface Ψ_0. So for flows with low enough mechanical energies, streamlines oscillate about the bottom of the potential well, which in full three-dimensional configuration space maps onto the two-dimensional initial flux surface.

https://doi.org/10.1017/S0022377808007666 Published online by Cambridge University Press

Discovering a necessary condition for detachment then becomes a case-by-case exercise depending on the static external field arrangement and the streamline under consideration. The process involves examining the two-dimensional effective potential associated with a particular Ψ_0 and finding the highest energy for which a closed equipotential curve enclosing the zero-energy equilibrium curve exists. As was noted above, the zero-energy equilibrium curve is traced out by Ψ_0. This highest-energy closed equipotential signifies the effective potential barrier that the hybrid particle must overcome to escape the well and travel off toward infinity, where $U_{\rm H}$ asymptotically falls to zero. The requisite escape energy and the shape of the potential barrier will vary depending on r_0, which determines Ψ_0. Hooper finds that this highest closed equipotential curve forms a separatrix denoting the spatial limits accessible to flows that are energetically constrained to follow confined paths [3]. Additionally, we observe from (3.1) that flows generated on the axis of symmetry always detach regardless of initial pitch angle, because the equilibrium flux surface extends out to infinity along the z-axis.

We now proceed to explore (2.9) in order to determine exhaust regimes that provide plume narrowing, exhaust aperture utilization, and overall detachment superior to initially field-directed exhaust flows. This translates to better efficiency and performance in a structurally unchanged thruster guide field. A highly varied set of flow behaviors can result from adjusting the initial injection conditions along the system boundary. The initial bulk mechanical rotation of the plasma is reflected in the values of $\Psi'_{\rm i0}$ and $\Psi'_{\rm e0}$.

The general effects of any rotational scheme are more easily recognized by recasting $U_{\rm eff}$ in a more physically intuitive form (cf. (2.11)). By expanding the squares, substituting the definitions for $\Psi'_{\alpha 0}$, and completing the squares, we get the result

$$U_{\rm eff} = \frac{e^2}{2(m_{\rm i}m_{\rm e})^{1/2}}\frac{1}{r^2}((\Psi_m - \Psi)^2 + \xi), \tag{3.2}$$

with

$$\Psi_m \equiv \Psi_0 + \frac{m_{\rm i}m_{\rm e}r_0^2}{e(m_{\rm i}+m_{\rm e})}(\dot\theta_{\rm i0} - \dot\theta_{\rm e0}), \tag{3.3}$$

and

$$\xi \equiv \frac{m_{\rm i}m_{\rm e}r_0^4}{e^2(m_{\rm i}+m_{\rm e})^2}(m_{\rm i}\dot\theta_{\rm i0} + m_{\rm e}\dot\theta_{\rm e0})^2. \tag{3.4}$$

Non-zero initial angular velocities for each plasma species then have two primary effects on $U_{\rm eff}$. First, we can shift the equilibrium flux surface, Ψ_m, away from Ψ_0 without shifting r_0. Second, since (3.4) illustrates that ξ is always positive, we can add a radially repulsive term with $1/r^2$ dependence. From (3.2) through (3.4), we get Hooper's familiar result for the effective potential, $U_{\rm H}$, in the limit of $\dot\theta_{\rm i0} = 0 = \dot\theta_{\rm e0}$ (cf. (3.1)) [3].

Before focusing on a specific magnetic guide field geometry, we can identify two general rules that should optimize the exhaust performance in any axisymmetric guide field. First, we note that the repulsive force provided by the ξ term is undesirable in any case where plume narrowing is a goal, as it largely serves to defocus the plume radially. Therefore, we suggest that an optimal regime would be one where $\xi = 0$, or

$$\frac{\dot\theta_{\rm i0}}{\dot\theta_{\rm e0}} = -\frac{m_{\rm e}}{m_{\rm i}}. \tag{3.5}$$

https://doi.org/10.1017/S0022377808007666 Published online by Cambridge University Press

Second, assuming the rotational constraint of (3.5), we recognize that for a particle starting on a flux surface Ψ_0, adding rotation such that $\Psi_m < \Psi_0$ will move the hybrid particle's equilibrium flux surface to a flux surface lying closer to the z-axis than the original. Thus the particle will initially experience a radial attraction inward toward the lower flux surface, and under the right conditions it will settle onto a path closer to the z-axis, resulting in a smaller plume angle. Interestingly, in the limit of $\Psi_m \to 0$, the equilibrium flux surface in the first term of (3.2) is moved to the z-axis, similar to the case of the particle starting on the symmetry axis in Hooper's limit, which always results in detachment due to the absence of any equipotential curves enclosing the equilibrium curve. Thus setting $\Psi_m \leqslant 0$ guarantees that the plasma will escape confinement by the field and detach, since the addition of an arbitrary repulsive ξ term would not lead to the formation of closed equipotentials. This result holds independent of the initial meridional velocity of the hybrid particle – it is a sufficient condition for detachment that trivially satisfies the necessary condition established above: since the effective potential in the $\Psi_m \to 0$ limit possesses no closed equipotential contours lying outside the equilibrium contour, which itself is not closed, then a hybrid particle with any non-zero initial velocity moving in the effective potential will travel off toward infinity.

4. Current loop guide field and simulation results

To demonstrate the positive effects of properly selected rotational profiles for the plasma species, we consider the example of a current ring guide field, which is also known as a physical dipole field. The exact field of a current ring involves multiple elliptic integrals, so we use an expansion of the magnetic vector potential to fourth order in the argument of the elliptic integrals to approximate the field of the current ring [5]; if the radius of the current ring is a, this expansion should represent sufficiently well the field of the current ring to within a distance of about $a/10$ from the current ring itself. We introduce the normalized coordinates $\rho \equiv r/a$ and $\zeta \equiv z/a$, and write the vector potential of the current ring as follows:

$$\mathbf{A} = \frac{\mu_0 I}{4\pi} \frac{\rho}{((\rho+1)^2 + \zeta^2)^{3/2}} \hat{\theta}. \tag{4.1}$$

The effective potential generated by this field for the r–z flow dynamics has the form

$$U_{\text{eff}} = U_0 \left(\frac{\Delta}{\rho} - \frac{\rho}{((\rho+1)^2 + \zeta^2)^{3/2}} \right)^2, \tag{4.2}$$

with

$$\Delta \equiv \frac{4\pi \Psi_m}{\mu_0 I a},$$

$$U_0 \equiv \frac{\mu_0^2 I^2 e^2}{32\pi^2 m_h},$$

and $m_h = (m_\text{i} m_\text{e})^{1/2}$. Note that we have assumed the optimal two-species angular velocity ratio from (3.5). Thus we find that U_{eff} is structurally modified by adjustment of the single parameter Δ, which scales with Ψ_m.

https://doi.org/10.1017/S0022377808007666 Published online by Cambridge University Press

We can gain a qualitative sense for how Δ affects the focusing of a streamline by solving (4.2) for ζ^2:

$$\zeta^2 = -(\rho+1)^2 + \frac{\rho^{4/3}}{(\Delta \pm (U_{\text{eff}}/U_0)^{1/2}\rho)^{2/3}}. \tag{4.3}$$

The plus sign corresponds to equipotential surfaces that reside within the equilibrium flux surface Ψ_m and are always closed, while the minus sign corresponds to equipotential surfaces lying outside the equilibrium flux surface. The latter equipotential surfaces represent the part of the potential landscape over which the hybrid particle must traverse in order to escape confinement. Each of these equipotential curves can be either entirely open or consist of one open curve and one closed curve, with a radial region in between where $\zeta^2 < 0$. Note that the equipotential where the associated open and closed curves intersect at the ζ^2-axis denotes the separatrix between open and closed contours—it is the highest closed contour, and thus it corresponds to the effective potential barrier that must be overcome for a hybrid particle to detach. In terms of (4.3), the separatrix occurs for the solution with a doubly degenerate root.

Taking the limit of (4.3) as $\rho \to [\Delta/(U_{\text{eff}}/U_0)^{1/2}]_-$ for a given U_{eff} results in $\zeta^2 \to \infty$. This means that the open portion of the equipotential corresponding to any value of U_{eff} asymptotically approaches this radial value as the axial coordinate goes to infinity. Furthermore, increasing U_{eff} for fixed Δ decreases the asymptotic value of ρ, and so this series of curves for fixed Δ portrays a sharply increasing potential slope as one nears the z-axis. In fact, for non-zero Δ, it is apparent from (4.2) that $U_{\text{eff}} \to \infty$ as $\rho \to 0$. It is this potential slope that tends to push the hybrid particle outward radially, causing plume divergence in the plasma flow. Here we once again confirm that choosing a small Δ, and hence a small Ψ_m, for any given streamline will flatten this potential slope near the z-axis, which in turn reduces the outward radial force experienced by the hybrid particle, allowing the streamline to asymptotically diverge at a significantly smaller angle.

A mathematically valid solution can only occupy a region in r–z space where all characteristic curves are non-intersecting, producing a laminar flow profile. Because (2.5) and (2.6) are quasilinear, the characteristic curves are uniquely defined and non-intersecting in the five-dimensional space defined by $(r, z, u_r, u_\theta, u_z)$, but the projections of the characteristic curves onto the two-dimensional r–z space can overlap. Intersecting characteristics lead to double-valued solutions, which is an unacceptable result for any steady-state flow field. Thus, in the case of intersecting characteristics, our model breaks down and cannot give an account of the plasma behavior. Only certain special radial rotational profiles will produce mathematically valid solutions, and the following analysis explores several such profiles.

Two physical quantities will be defined for each flow profile: the exhaust aperture fraction and the plume angle. We define the exhaust aperture fraction, A_{exh}, as the fraction of the total exhaust aperture cross-sectional area through which laminar, directed flow is possible, with directed flow defined as flow with an escape angle of less than 45° off the z-axis. The plume angle, α, is the maximum escape angle of any streamline in a given thruster regime, with a maximum allowed value of 45°. Larger A_{exh} and smaller α result in higher mass flow rate and axial specific impulse, resulting in a marked performance increase.

Our baseline reference will be a standard flow plot for a plasma with no rotation. We will model an argon-electron plasma ($m_h = 2.469 \times 10^{-28}$ kg) flowing through

https://doi.org/10.1017/S0022377808007666 Published online by Cambridge University Press

a current ring of radius $a = 0.05$ m with a guide field that measures 0.1 T at the origin. The analysis can be scaled for any set of parameter values, but we choose these values to demonstrate the experimental relevance of the results and to follow closely with simple examples pursued by Hooper. A typical exhaust velocity is of the order 10^5 m s^{-1}, which we take to be field-directed in the $z = 0$ plane with no initial azimuthal velocity. The streamlines in the r–z plane are depicted in Fig. 1(a). Directed flow occurs only for plasma originating at $\rho < 0.5$. Furthermore, for $\rho > 0.7$ the streamlines begin to overlap and the solutions along the outer characteristics become invalid. We thus obtain directed flow through an exhaust aperture fraction $A_{\rm exh}$ of 0.25, with a plume angle α of the maximum 45°.

In Fig. 1(b), a uniform flux-cancellation regime with $\beta = 0.94$ has been modeled. A flux-cancellation value of β simply means that, at each radial position, Ψ_m is selected such that $\Psi_m(r_0) = (1 - \beta)\Psi_0(r_0)$, with Ψ_m defined according to (3.3) and (3.5). The field-directed initial flow velocity is still 10^5 m s^{-1}, but this time the plasma is also given an initial azimuthal velocity profile. In this regime, the directed flow originates from an annular region near the outside of the exhaust aperture, yielding a nearly doubled $A_{\rm exh} = 0.44$ with a much-reduced plume angle of 29°. After further numerical runs we find that a slightly lower β yields a lower α at the cost of a lower $A_{\rm exh}$. For $\beta = 0.90$, we have $A_{\rm exh} = 0.39$ and $\alpha = 26°$, and for $\beta = 0.85$, we have $A_{\rm exh} = 0.29$ and $\alpha = 20°$. Thus, even for $\beta = 0.85$ we still have a better $A_{\rm exh}$ than the no-rotation regime with α reduced by 55%. One interesting feature to note is that these uniform flux-cancellation regimes impart initial angular velocities on each of the constituent plasma particles of the same order as each particle's local gyrofrequency. The case where the initial angular velocity profile exactly matches the local gyrofrequency is depicted in Fig. 2. This scenario yields the largest $A_{\rm exh}$ yet, at a value of 0.56, with $\alpha = 39°$, which is still an improvement over the no-rotation case.

For a more global perspective of the possible solution space, we include contour plots depicting the escape angles and averaged r–z trajectory curvatures over a wide expanse of R_0–P_θ phase space. Well-behaved laminar velocity profiles will have escape angles increasing monotonically with R_0 as well as relatively low trajectory curvatures in the r–z plane, which helps select paths that do not oscillate wildly and intersect other streamlines. Figure 3(a) depicts the streamline escape angle, in degrees, versus the initial phase space variables, while Fig. 3(b) depicts the averaged r–z trajectory curvatures over the same domain in phase space. R_0–P_θ curves have been included that denote each of the three regimes examined above. Figure 3 reinforces the results from our specific examples: the paths with simultaneously small escape angles and small trajectory curvatures occupy the part of phase space corresponding to larger initial radial positions and lower initial P_θ, i.e. lower initial Ψ_m, as was predicted in the last section.

5. Discussion

Any thruster utilizing a magnetic field near the exhaust port must satisfy the criteria for magnetized plasma detachment to function properly. Such thrusters include electromagnetic thrusters, notably various forms of magnetoplasmadynamic thrusters [6], as well as electrothermal thrusters such as the variable specific impulse magnetoplasma rocket (VASIMR) and the Helicon Double-Layer Thruster (HDLT), which both use strong magnetic fields to guide the plasma to the exhaust

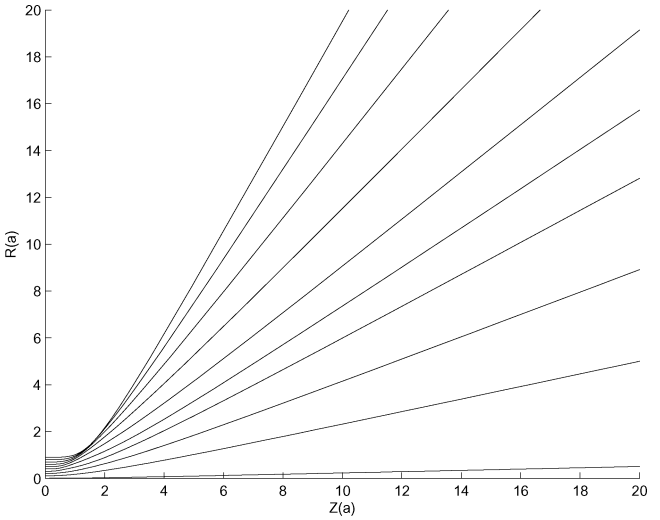

(a)

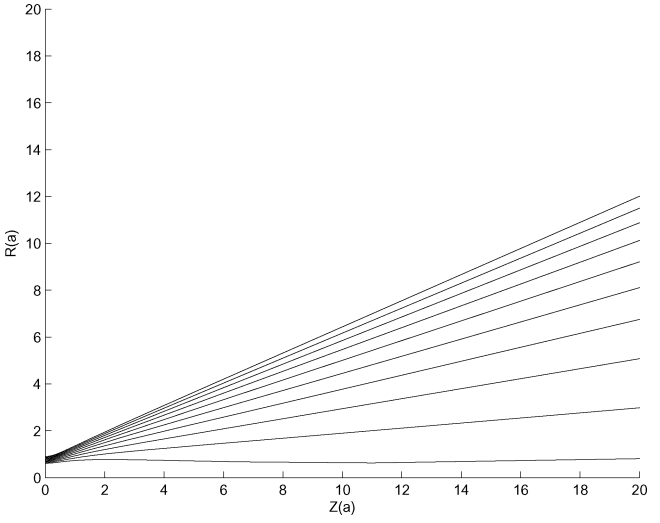

(b)

Figure 1. (a) Streamlines with no rotation, $A_{\mathrm{exh}} = 0.25$ for $\alpha = 45°$. (b) Streamlines for the 0.94 flux-cancellation profile, $A_{\mathrm{exh}} = 0.44$ for $\alpha = 29°$.

port [7–9]. Our model provides a correction to Boswell's analysis of single-ion detachment dynamics in the HDLT [4]. Having neglected ambipolar effects and limited dynamical considerations to the calculation of single-ion trajectories in the vacuum magnetic field, the downstream beam size was underestimated by approximately 10%, suggesting the presence of defocusing ambipolar drift effects in the experiment that were not effectively characterized by the simplified single-ion model. To obtain a correction to Boswell's results for the initially axially directed

https://doi.org/10.1017/S0022377808007666 Published online by Cambridge University Press

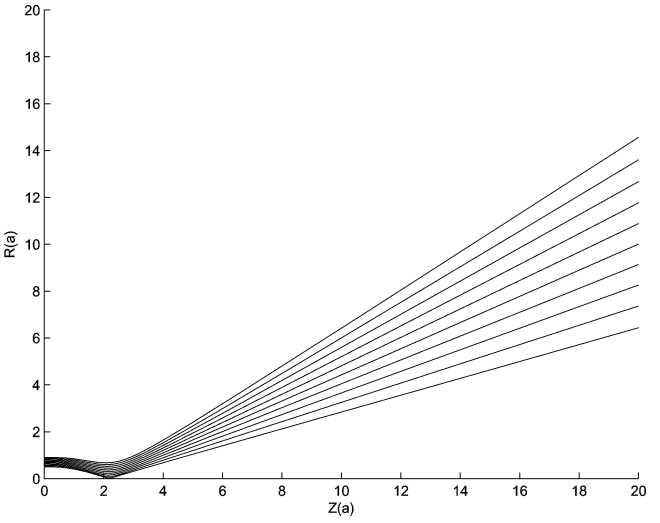

Figure 2. Streamlines for local gyrofrequency profile. $A_{\mathrm{exh}} = 0.56$ for $\alpha = 39^{\circ}$.

ion flow, (3.1) suggests that the ion mass be replaced by the effective hybrid mass, i.e. $m_{\mathrm{i}} \rightarrow m_h$, while the equations of motion are left structurally unchanged. Since the hybrid mass is smaller than the ion mass, the size of the beam envelope will increase accordingly due to the more pronounced impact of the field curvature on the hybrid particle trajectories.

Our model can also be used to describe plume dynamics in thrusters using magnetic fields close to the exhaust port for reasons other than guiding the main plasma exhaust plume. For instance, the cylindrical Hall thruster uses an expanding magnetic field near the exhaust opening to trap electrons in the virtual cathode segment of the thruster [10,11]. Unlike VASIMR and HDLT, ions in the cylindrical Hall thruster are unmagnetized. However, the confinement of the electrons in the magnetic field and the observed quasineutrality in the exhaust plume ties the massive ions to the lighter electrons and inhibits magnetized plasma detachment. Thus, ambipolar detachment provides an account for how the electron confinement leads to divergence in the plasma exhaust plume. Fruchtman and Cohen-Zur [12] have provided a limiting planar model of a Hall thruster, which suggests that placing the ionization layer near the magnetic field null surface will lead to a focusing effect in the plume downstream. This corresponds to the limit of $\Psi_m \rightarrow 0$ in our model, which as we have shown tends to provide a focusing effect in the downstream plume dynamics of any axisymmetric thruster configuration. It should be noted, however, that Fruchtman and Cohen-Zur's model additionally accounts for ion acceleration in the electron virtual cathode, whereas our model assumes a plasma with a fixed flow energy.

While adding rotational profiles to exhaust plumes can optimize thruster performance, one concern is how rotating plasmas can be produced in practice. We will provide a brief existence argument by considering a few different methods. The following methods assume that we have a plasma source providing a cold, neutral plasma column flowing axially along a z-directed uniform magnetic field at some uniform fluid velocity. The first method is passive and involves passing the plasma column through an abrupt step in the magnetic field at some z, where the

https://doi.org/10.1017/S0022377808007666 Published online by Cambridge University Press

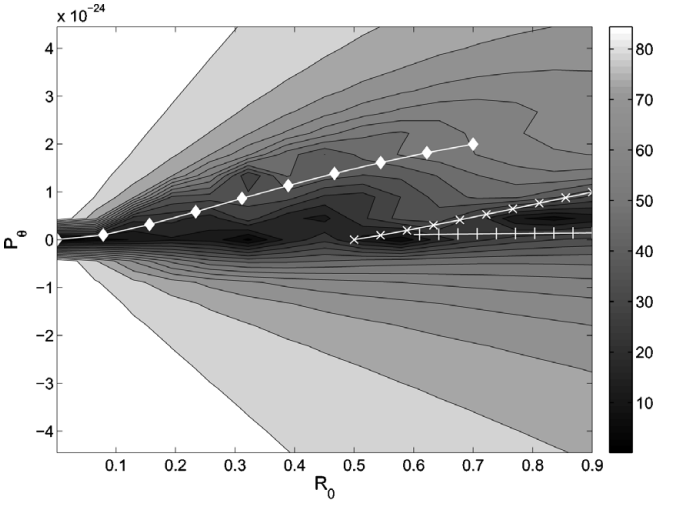

(a)

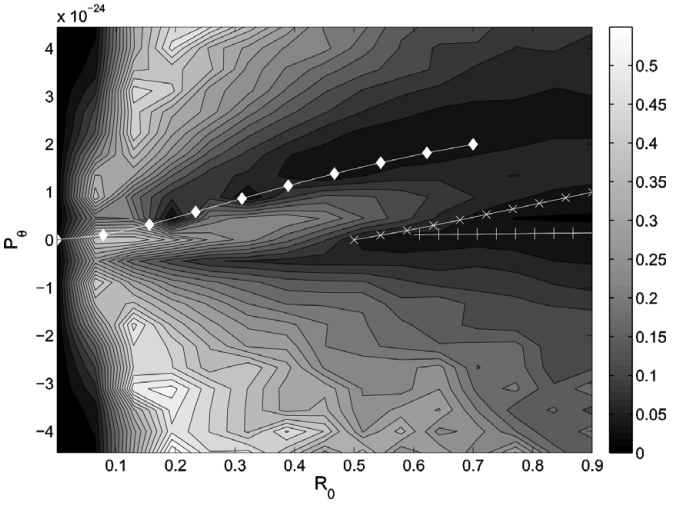

(b)

Figure 3. (a) Escape angle (in degrees) versus. initial R and P_θ. (b) Averaged r–z curvature of trajectories versus initial R and P_θ. Diamonds correspond to no rotation, crosses correspond to the local gyrofrequency regime, and pluses correspond to the $\beta = 0.94$ regime.

field quickly shifts to a new magnitude, and possibly a new sign, on the other side of the step. The assumption is that the step is sufficiently abrupt so that neither species is significantly deflected in the radial direction as it crosses the step, and so by conservation of canonical P_θ (cf. (2.6)) each species acquires a bulk azimuthal velocity given by

$$u_{\alpha\theta} = -\frac{q_\alpha(\Psi_\mathrm{f} - \Psi_\mathrm{i})}{m_\alpha r}, \tag{5.1}$$

https://doi.org/10.1017/S0022377808007666 Published online by Cambridge University Press

where we have assumed that the flow started with no azimuthal velocity. Note that the final angular velocities of electrons and ions at the same radial position will scale exactly with the ideal ratio for minimally defocused flow identified in (3.5). Theiss et al. demonstrated that this method could be used to establish the correct bulk rotational equilibrium flow supported in a pure electron plasma [13], but this technique could also be used with neutral plasmas to generate rotation in both species simultaneously.

While the step does not introduce any extra energy into the flow, it does permit reallocation of some of the axial flow energy into azimuthal flow to produce the most focused and efficient flow downstream. Once the plasma is many exhaust aperture radii a away from the exhaust port, the magnetic field falls asymptotically to zero and the neutral flow becomes approximately free streaming. Thus, all of the axial energy that had been converted into azimuthal energy once again becomes purely meridional energy, except now the flow is better focused, yielding a higher specific impulse for a given flow energy.

There also exist active methods for generating rotation in axially confined columnar plasmas. One method utilizes high-frequency electromagnetic waves to establish a radial ponderomotive force profile in the plasma column [14], which then acts with the axial magnetic field to induce azimuthal drift motion in both plasma species. On the other hand, resonant high-frequency radiofrequency fields could also be used to heat up one or both of the plasma species and establish a radial pressure profile, which in turn drives an azimuthal current in order for the plasma to maintain steady-state equilibrium.

6. Summary

We have extended the analysis of Hooper's ambipolar detachment scheme to include plasma flows possessing unique initial azimuthal velocity profiles for each plasma species. In doing so we have demonstrated that fine-tuning the initial azimuthal velocity profiles at the boundary of the exhaust system can significantly affect the downstream dynamics of the plume, allowing one to simultaneously narrow the plume, enhance magnetized plasma detachment, and utilize more exhaust aperture area without having to structurally change the applied magnetic guide field. A specific example of an approximated current ring guide field was used to illustrate the beneficial effects of certain rotational profiles, which include a reduction of the plume angle by more than 50% and an increase in exhaust aperture utilization of more than 100%. Finally, an existence argument for the production of axially flowing, rotating plasmas was given.

Acknowledgements

The authors thank Ilya Dodin, Jean Marcel Rax, and Andrey Zhmoginov for useful discussions. This work was supported by US DoE contract No. DE-AC02-76-CH03073. One of us (PFS) was supported by the National Defense Science and Engineering Graduate Fellowship.

References

[1] Breizman, B. N., Tushentsov, M. R. and Arefiev, A. V. 2008 *Phys. Plasmas* **15**, 057103.

[2] Arefiev, A. V. and Breizman, B. N. 2005 *Phys. Plasmas* **12**, 043504.
[3] Hooper, E. B. 1993 *J. Propul. Power* **9**, 757.
[4] Gesto, F. et al. 2006 *J. Propul. Power* **22**, 24.
[5] Smythe, W. R. 1950 *Static and Dynamic Electricity*, 2nd edn. New York: McGraw-Hill.
[6] Krülle, G. et al. 1998 *J. Propul. Power* **14**, 754.
[7] Chang-Díaz, F. R. 2000 *Sci. Amer.* **283**, 90.
[8] Squire, J. P. et al. 2003 *Trans. Fusion Technol.* **43**, 111.
[9] Charles, C. and Boswell, R. W. 2003 *Appl. Phys. Lett.* **82**, 9.
[10] Raitses, Y. and Fisch, N. J. 2001 *Phys. Plasmas* **8**, 2579.
[11] Smirnov, A., Raitses, Y. and Fisch, N. J. 2007 *Phys. Plasmas* **14**, 057106.
[12] Fruchtman, A. and Cohen-Zur, A. 2006 *Appl. Phys. Lett.* **89**, 111501.
[13] Theiss, A. J., Mahaffey, R. A. and Trivelpiece, A. W. 1975 *Phys. Rev. Lett.* **35**, 1436.
[14] Motz, H. and Watson, C. J. H. 1967 *Adv. Electron.* **23**, 153.